NUMERICAL SIMULATION AND EXPERIMENTS OF HYDROGEN DIFFUSION BEHAVIOR FOR FUEL CELL ELECTRIC VEHICLE

Matsumoto, M.[1] and Shimizu, K.[1]
[1] Honda R&D Automobile R&D Center, 4630 Shimotakanezawa, Hagamachi, Hagagun, Tochigi, 321-3393, Japan, Mitsunori_Matsumoto@n.t.rd.honda.co.jp

ABSTRACT

Research was conducted on hydrogen diffusion behavior to construct a simulation method for hydrogen leaks into complexly shaped spaces such as around the hydrogen tank of a fuel cell electric vehicle (FCEV). To accurately calculate the hydrogen concentration distribution in the vehicle underfloor space, it is necessary to take into account the effects of hydrogen mixing and diffusion due to turbulence. The turbulence phenomena that occur in the event that hydrogen leaks into the vehicle underfloor space were classified into the three elements of jet flow, wake flow, and wall turbulence. Experiments were conducted for each turbulence element to visualize the flows, and the hydrogen concentration distributions were measured. These experimental values were then compared with calculated values to determine the calculation method for each turbulence phenomenon. Accurate calculations could be performed by using the k-ω Shear Stress Transport (SST) model for the turbulence model in the jet flow calculations, and the Reynolds Stress Model (RSM) in the wall turbulence calculations. In addition, it was found that the large fluctuations produced by wake flow can be expressed by unsteady state calculations with the steady state calculation solutions as the initial values. Based on the above information, simulations of hydrogen spouting were conducted for the space around the hydrogen tank of an FCEV. The hydrogen concentration calculation results matched closely with the experimental values, which verified that accurate calculations can be performed even for the complex shapes of an FCEV.

1. INTRODUCTION

Honda has positioned mobility using hydrogen energy as the ultimate low-carbon technology, and is actively developing FCEV, Solar Hydrogen Stations (SHS) and other technology (Fig. 1). Hydrogen sensors are mainly used in FCEV to detect possible hydrogen leaks (Fig. 2). Efficient detection using few hydrogen sensors is the ideal situation when designing FCEV and other applications. However, the spaces around parts that hold hydrogen have complex shapes due to floor panels, devices, piping, wiring and other items, and it is a challenge to understand the diffusion behavior of hydrogen leaks. Therefore, Computational Fluid Dynamics (CFD) is thought to be a promising method for simulating hydrogen diffusion, and efforts have been made to construct models that can accurately calculate hydrogen diffusion in spaces that reflect CATIA model shapes.

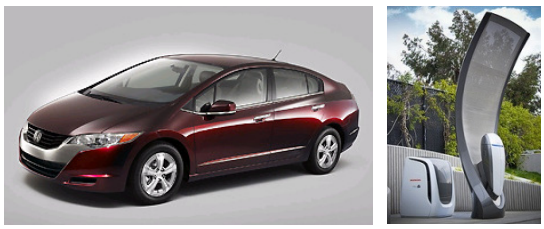

Figure 1. FCX Clarity (left) and SHS (right)

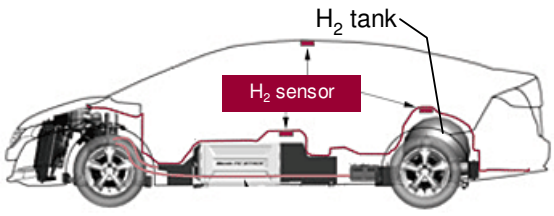

Figure 2. Position of hydrogen sensors

2. TYPES OF HYDROGEN FLOWS IN THE VEHICLE UNDERFLOOR SPACE

In the event that hydrogen leaks into the vehicle underfloor space, the hydrogen is thought to flow and diffuse according to the phenomena shown in Fig. 3. First, jet turbulence that involves compression is formed at the leak point, and the hydrogen diffuses while rolling up the surrounding air. When there are objects such as piping or wiring in the hydrogen flow path, wake (downstream) turbulence is generated to the rear of these objects. In addition, the hydrogen flows along the vehicle floor panels and the wall surfaces of the tank and other large structures, and the behavior transitions to flow and diffusion resulting from wall turbulence due to the effects of the wall surface viscosity. As the flow progresses, the inertia force of the spouting weakens, and the effects of buoyancy become relatively dominant, so the hydrogen rises and remains in the upper space.

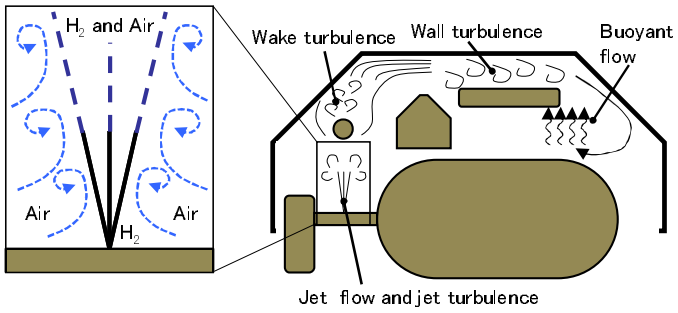

Figure 3. Flow phenomena in case of a hydrogen leak in the vehicle underfloor space

Of the diffusion phenomena within a flow field, the effects of turbulent diffusion and mixing whereby mixing is induced by turbulence are more dominant than the effects of molecular diffusion due to differences in concentration. Therefore, to simulate hydrogen diffusion in the vehicle underfloor space, it is thought important to accurately calculate each turbulence element of jet flow, wake flow, and wall turbulence.

3. LEAK PRESSURE AND FLOW RATE RANGE

In an FCEV that carries compressed hydrogen, the hydrogen in the tank is instantly decompressed by a regulator at the tank outlet. Therefore, the hypothetical pressure range for hydrogen leaks was set as the several MPaG or less used by the fuel system after decompression.

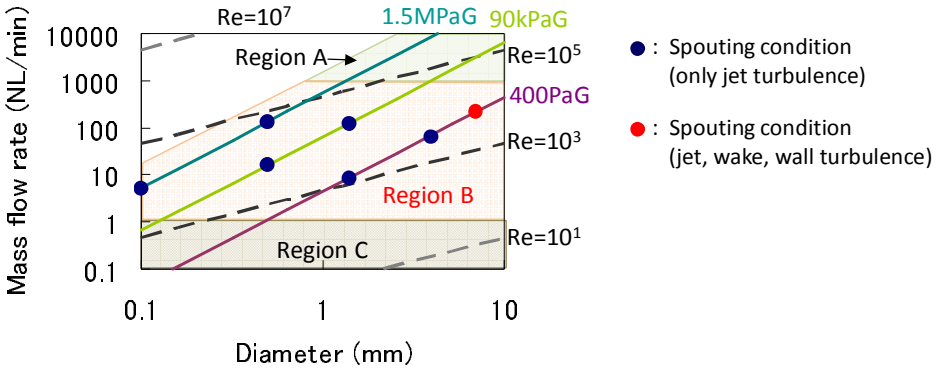

Figure 4. Spouting conditions

Figure 4 shows the relationship at each pressure in the case of hydrogen, with the nozzle diameter D on the horizontal axis and the mass flow rate M on the vertical axis. When hydrogen leaks at a

medium flow rate between Region A and Region C (Region B), it is a challenge to predict whether the spouting momentum or the buoyancy effects is dominant, and it is also a challenge to detect the drop in the pressure values inside the fuel system. Therefore, the hypothetical flow rate range was set at the several NL/min to several hundred NL/min of Region B.

The seven different spouting conditions indicated by the blue and red dots in Region B were set to investigate the jet turbulence calculation method. The spouting condition of the red dot was used to investigate the wake and wall turbulence calculation methods. These details are described in 4.1.1, 4.2.1 and 4.3.1.

4. DETERMINATION OF CALCULATION METHODS THROUGH EXPERIMENTS FOR EACH TURBULENCE ELEMENT

4.1 Jet Flow

4.1.1 Condition settings

Jet turbulence is generally expressed by the Reynolds number Re shown in Eq. (1), using the spout diameter D as the typical length, and the flow velocity U at the spout as the typical flow velocity.

$$\mathrm{Re} = \frac{\rho U D}{\mu} \tag{1}$$

where ρ is the density at the spout and μ is the dynamic viscosity.

The seven different conditions in the Reynolds number range of 10^3 to 10^5 shown in Fig. 4 were set by varying the spout diameter with respect to the three different nozzle upstream pressures of 1.5 MPaG which is higher than the choke pressure, 90 kPaG which is equal to the choke pressure, and 400 PaG (spouting flow velocity 100 m/s) which is lower than the choke pressure. The spouting direction was set as vertically upward.

4.1.2 PIV measurement

Among the spouting conditions set in 4.1.1, Particle Image Velocimetry (PIV) measurement was performed using helium for the 400 PaG condition, and the flow characteristics were visualized. The ratio of the coefficients of kinematic viscosity μ/ρ of hydrogen and helium is approximately 1.2, so the Reynolds numbers of hydrogen and helium differ by only approximately 1.2 times given the same diameter and flow velocity. Therefore, turbulence phenomena can be roughly understood even when the hydrogen is replaced with helium for measurement.

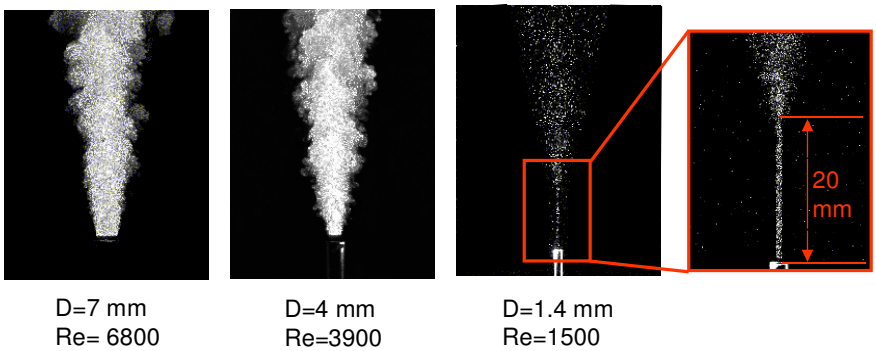

Figure 5. Visualized images of jet flows

Figure 5 shows the visualized images of the flows obtained by PIV measurement. Under the Reynolds number 3900, D = 4 mm and Reynolds number 6800, D = 7 mm conditions, turbulence

occurs and the flow spreads outward starting from the spout. However, under the Reynolds number 1500, D = 1.4 mm condition, a laminar flow state exists for approximately 20 mm after spouting. This indicates that laminar-turbulent transition occurs at the nozzle at a Reynolds number of around 1500.

4.1.3 Hydrogen concentration measurement

The hydrogen concentrations on the spouting axis were measured for the seven spouting conditions set in 4.1.1. The HX-07i ion detector (made by NOHMI BOSAI LTD.) was used as the hydrogen concentration sensor [1]. The hydrogen concentration on the spouting axis of a hydrogen jet flow from a circular opening is expressed by the approximation shown in Eq. (2) [2].

$$C = a_1\left(\frac{x}{\theta}\right)^{-1} \quad , \quad \theta = D\sqrt{\frac{\rho}{\rho_a}} \tag{2}$$

where, ρ_a is the air density, a_1 is the proportional constant (4600 to 5200) and x is the distance from the spout. The applicable range of this approximation is x/θ = 200 to 1000.

Figure 6 shows the experiment results plotted logarithmically in both directions, with x/θ on the horizontal axis and the hydrogen concentration on the vertical axis. It can be said that the diffusion phenomena is described well by Eq. (2) when the Reynolds number is sufficiently larger than 1500. However, under the D = 1.4 mm, P = 400 PaG condition, a laminar flow area approximately 20 mm long exists immediately after the spout, so this case differs from the other spouting conditions, and deviates from the straight line with a slope of -1.

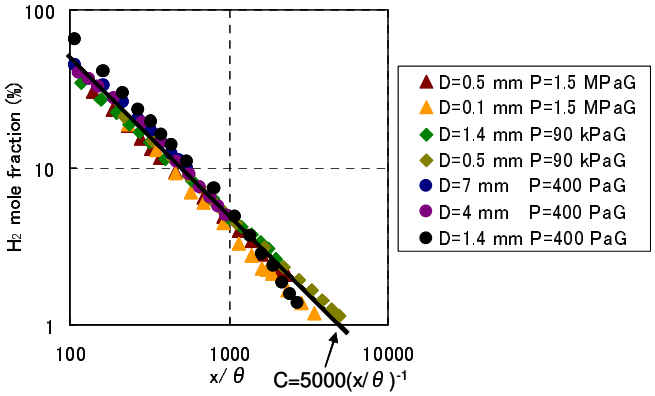

Figure 6. Experiment results of hydrogen concentration on spouting axis during jet flow

4.1.4 Simulation method

There are numerous methods for calculating turbulence, but in consideration of application to FCEV design, it is preferable that calculations can be performed using the Reynolds Averaged Navier-Stokes (RANS) model, which has a low calculation load. Therefore, five different turbulence models with proven results for engineering calculations were taken as candidates, and the calculation accuracy was verified. FLUENT6.3 was used as the solver in the calculations below.

First, the hydrogen concentrations on the spouting axis calculated by each turbulence model were compared with the measured values for the D = 1.4 mm, P = 90 kPaG spouting condition. The calculations used the steady-state calculation results, and the measured values used the time-averaged values of the saturation concentration. Figure 7 shows that the k-ω SST model is the most accurate. In the jet calculations, the high-speed free jet area and the area near the spout wall surface were calculated simultaneously. The k-ω SST model is thought to be accurate because it calculates spaces distant from the spout wall surface using the k-ε standard model that is suited to calculating free shear flow, and spaces near the spout wall surface using the k-ω standard model that does not

require modeling using a wall function.

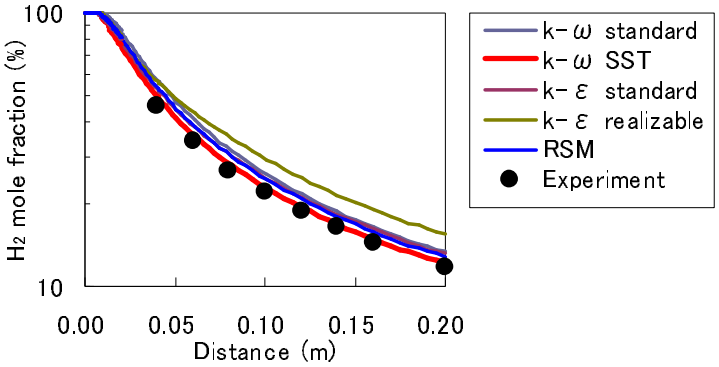

Figure 7. Comparison of calculations with experiment to determine the jet turbulence model

Values calculated by the k-ω SST model were also compared with the measured values for the other spouting conditions. Figure 8 shows that the k-ω SST model could perform accurate calculations regardless of the spouting conditions. As described in 4.1.3, the diffusion phenomena due to turbulence do not change greatly even with different spouting conditions, so the k-ω SST model is thought to be universally effective.

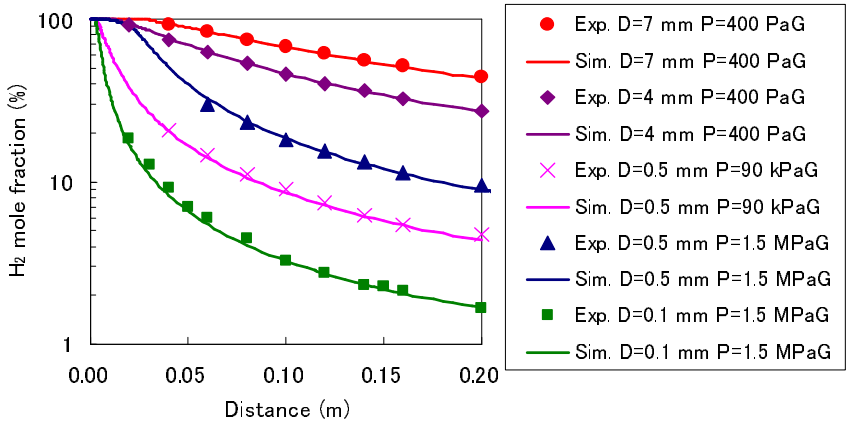

Figure 8. Comparison of calculated and measured values for hydrogen concentration under various spouting conditions

Regarding the D = 1.4 mm, P = 400 PaG condition that has a 20 mm laminar flow area immediately after the spout, it was found that shifting the calculation results by x = 20 mm provided a close match with the measured values (Fig. 9).

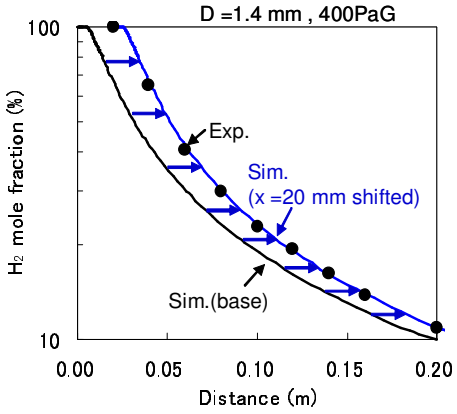

Figure 9. Comparison of calculated values shifted by 20 mm and measured values

4.2 Wake Flow

4.2.1 Condition settings

The wake turbulence generated to the rear of a 20 mm diameter pipe was used as the subject, on the assumption of piping and wiring in the vehicle underfloor space. The spouting conditions were a spout diameter 7 mm and pressure of 400 PaG, and the pipe was installed on the spouting axis 0.1 m directly above the spout. The flow velocity at the pipe was approximately 20 m/s, and the hydrogen concentration was approximately 65%. The Reynolds number obtained using the pipe diameter as the typical length and the flow velocity at the pipe as the typical flow velocity was approximately 20000.

4.2.2 PIV measurement

PIV measurement was performed using helium in the same manner as the jet flow measurement. Figure 10 shows the visualized images of the flows. Compared with the free jet flow, the phenomenon was confirmed where the flow to the rear of the pipe wavered greatly over time. In addition, Fig. 11 compares the flow velocity values on the spouting axis with the free jet flow case. This confirmed that the flow velocity decreased to the rear of the pipe.

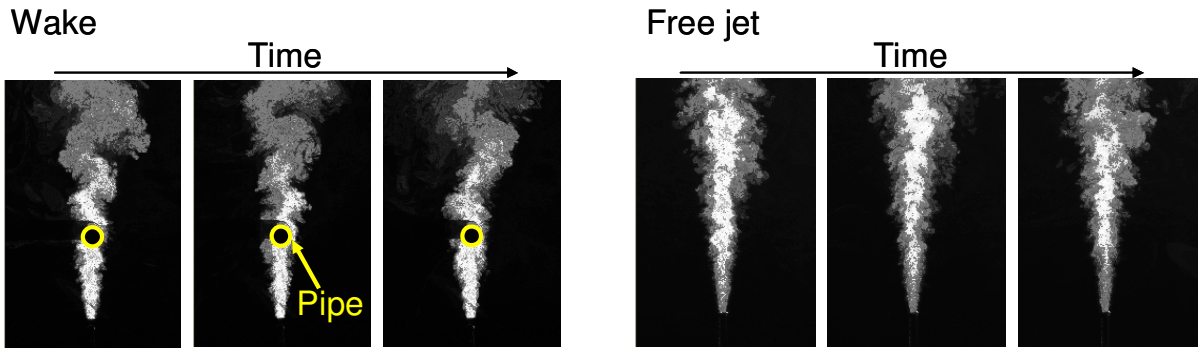

Figure 10. Comparison of wake flow and jet flow using visualized images (photographs)

4.2.3 Hydrogen concentration measurement

The effect of wavering to the rear of the pipe described in 4.2.2 on the hydrogen concentration was measured using a hydrogen sensor in the same manner as the jet flow measurement. Figure 12 shows the results. Compared with the free jet flow, a drop in the hydrogen concentration thought to be the effect of diffusion due to wake flow was observed from x = 0.14 m onward.

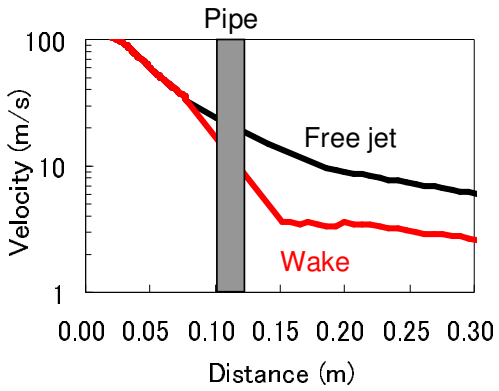

Figure 11. Comparison of flow velocity on spouting axis for wake flow and jet flow

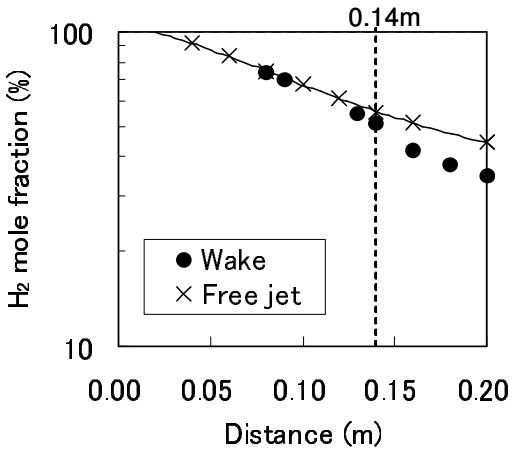

Figure 12. Comparison of hydrogen concentration on spouting axis for wake flow and jet flow

4.2.4 Simulation method

The steady-state calculation results using the five different RANS turbulence models were compared with the measured values in the same manner as for jet flow. Figure 13 shows the results. Among the candidate turbulence models, the RSM model was closest to the measured values, but the drop in concentration to the rear of the pipe could not be adequately expressed.

It was thought that the steady-state calculation results do not adequately express the time-averaged values of the strongly unsteady-state wake flow wavering confirmed in 4.2.2 and 4.2.3. Therefore, a method was attempted that consists of performing unsteady-state calculations using the steady-state calculation results as the initial values, and then averaging those results. A strongly wavering flow is thought to be a state in which multiple convergent solutions exist for the calculations. This method expresses wavering by transitioning between multiple convergent solutions over time, using the numerical error that occurs in the unsteady-state calculations as the starting point. A similar method is also used in reference [3], and its effectiveness for cases with large wavering is demonstrated.

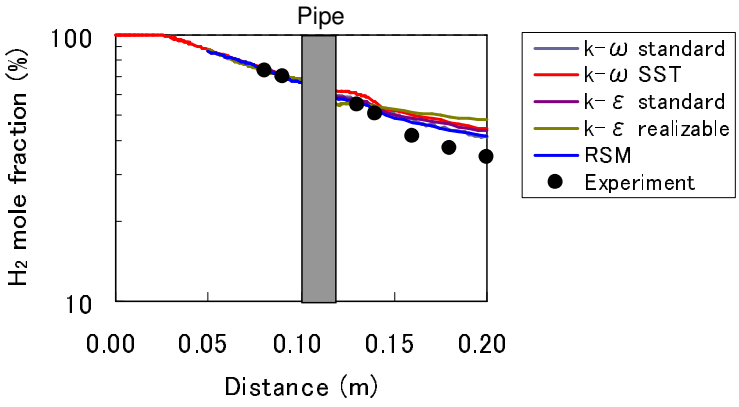

Figure 13. Comparison of calculations with experiment to determine the wake turbulence model

Figure 14 shows the unsteady-state calculation results. Wavering phenomena similar to the flows

observed by PIV measurement are expressed. In addition, Fig. 15 shows the results of comparing the averaged values of the unsteady-state calculations with the experimental values. This shows that unsteady-state calculations are able to express the drop in concentration to the rear of the pipe that could not be expressed by steady-state calculations.

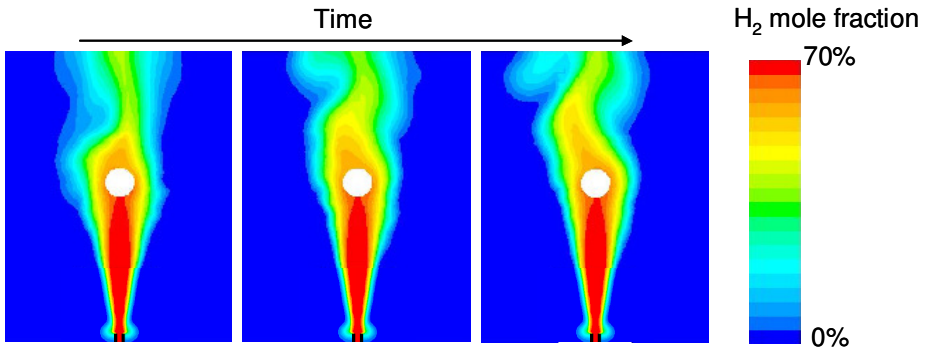

Figure 14. Hydrogen mole fraction contours obtained by unsteady-state calculations

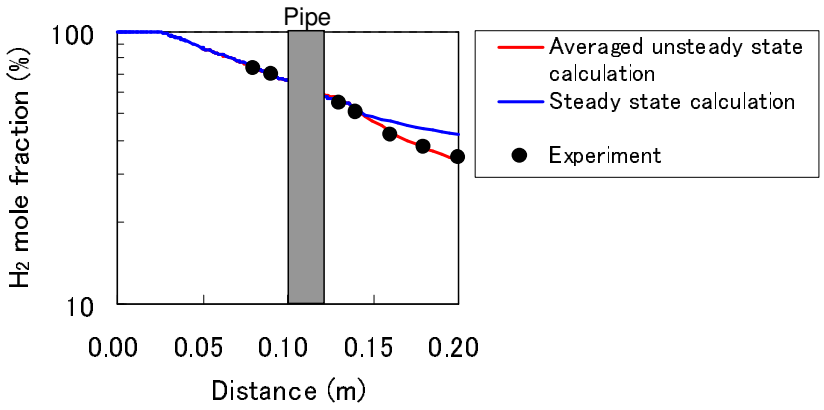

Figure 15. Accuracy enhancement effects of averaged unsteady-state calculation method

4.3 Wall Turbulence

4.3.1 Condition settings

The case with hydrogen spouting at a pressure of 400 PaG from a spout of diameter 7 mm parallel to the bottom side of a horizontal wall surface was investigated, on the assumption of flow along the bottom side of a vehicle floor panel.

4.3.2 PIV measurement

PIV measurement was performed using helium in the same manner as the jet flow and wave flow measurements. Wall turbulence was measured in the two planes parallel and perpendicular to the wall surface. Regarding measurement in the plane parallel to the wall surface, the theoretical flow velocity on the wall surface is zero, so the plane 7 mm below the wall surface was measured. Figure 16 shows the results. This shows that the flow velocity distribution in the direction parallel to the wall surface spreads approximately five times wider than the flow velocity distribution in the direction perpendicular to the wall surface.

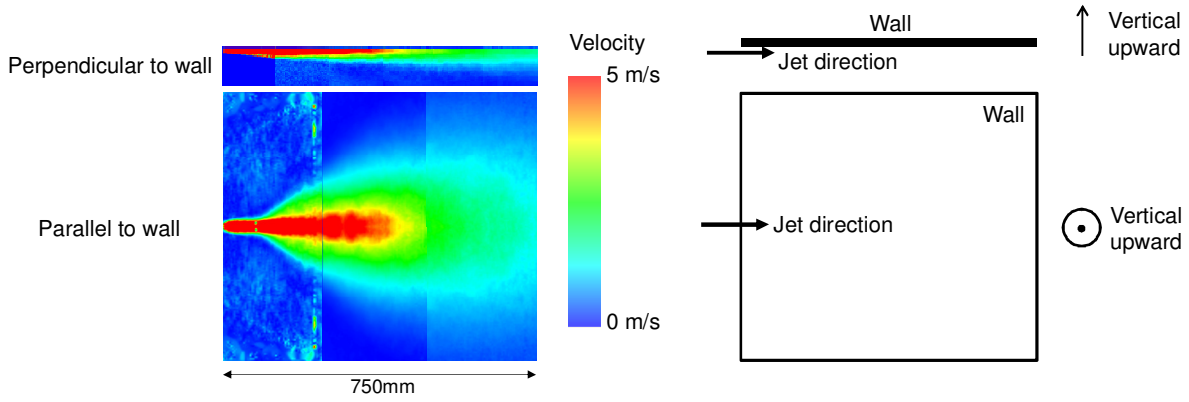

Figure 16. PIV measurement results of flow velocity distribution for wall turbulence

4.3.3 Hydrogen concentration measurement

Figure 17 shows the results of measuring the hydrogen concentration on the spouting axis. In addition, Fig. 18 shows the results of measuring the hydrogen concentration in the direction parallel to the wall surface at the point 0.4 m from the spout. Compared to the free jet flow, the hydrogen concentration of the wall turbulence on the spouting axis drops slower, and flow behavior with high concentrations spread over a wide range was also confirmed in the horizontal direction.

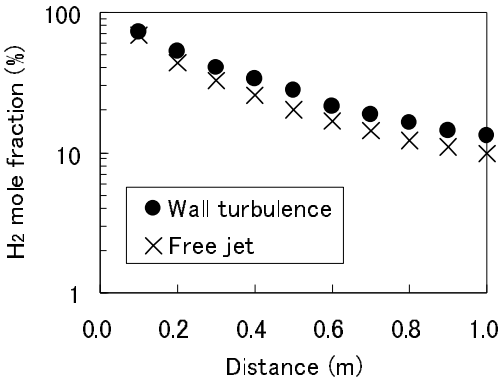

Figure 17. Comparison of hydrogen concentration on spouting axis for wall turbulence and jet flow

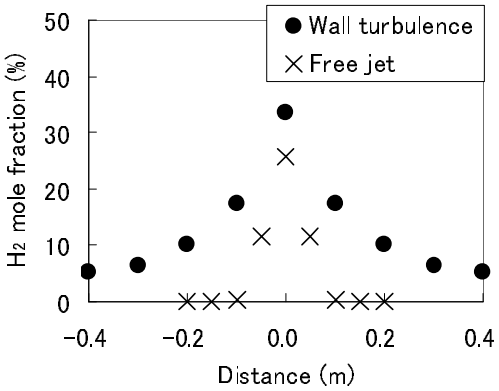

Figure 18. Hydrogen concentration spread for wall turbulence and jet flow

4.3.4 Simulation method

Calculations were performed for the five different RANS turbulence models in the same manner as for jet flow and wake flow, and the hydrogen concentration on the spouting axis and the flow velocity and spread of the hydrogen concentration in the direction parallel to the wall surface were verified. The calculations used the analysis region partitioning method introduced in reference [2] to lower the calculation load. The analysis region was divided at the point 0.14 m from the spout. The side closer to the spout was calculated by the k-ω SST model which is effective for jet flow calculations, and that calculation result was used as the boundary condition to calculate the side farther from the spout by the respective turbulence models. Figure 19 compares the hydrogen concentrations, and Fig. 20 shows contour diagrams of the velocity in the plane parallel to the wall surface.

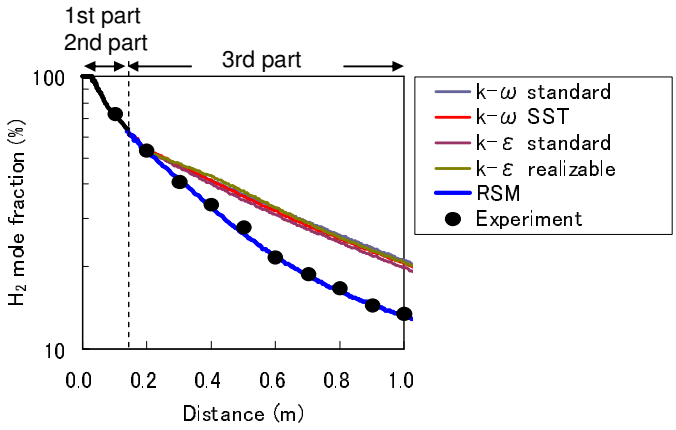

Figure 19. Comparison of calculations with experiment to determine the wall turbulence model

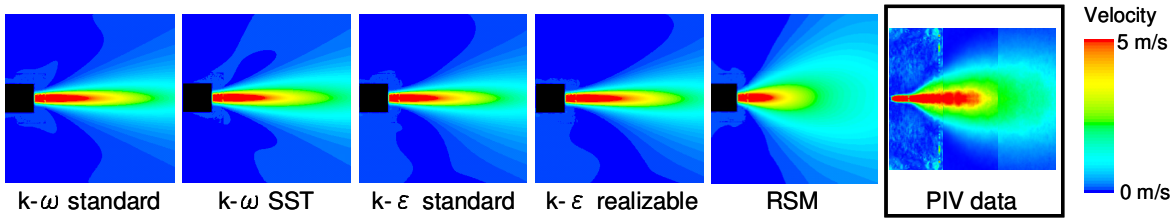

Figure 20. Velocity contours in plane parallel to wall surface

Only the RSM model, which is a seven-equation model, was able to express the behavior where the hydrogen concentration spreads out along the wall surface, and this model also accurately calculated the hydrogen concentration on the spouting axis. Longitudinal vortices with strong anisotropy are known to develop near the wall surface [4], and it is thought that the RSM model can effectively calculate the anisotropy of these vortices.

5. APPLICATION TO VEHICLE SHAPES

5.1 Condition Settings

Experiments and calculations were performed to verify the calculation time and calculation accuracy, using the subject of the vehicle underfloor space around the hydrogen tank in an FCEV in the initial development stage. The spouting condition was a spout diameter of 1.4 mm and pressure of 400 PaG. The spout was set near the piping joint on the side of the hydrogen tank, and hydrogen was spouted in the vertically upward direction. The spouting time was set at 7.2 s. Figure 21 shows the hydrogen spouting position and hydrogen concentration measurement position.

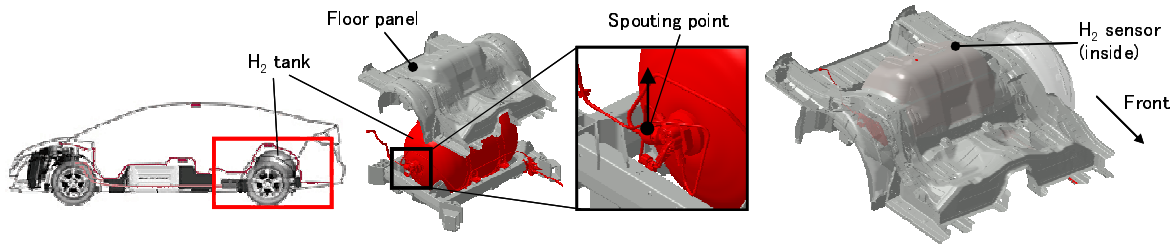

Figure 21. Model used for experiment

5.2 Calculation Methods

FLUENT6.3 was used as the solver, and the calculations were performed using the SIMPLE algorithm. A three-part partitioning calculation method, which is developed based on the conventional analysis region partitioning method, was used to shorten the calculation time (Fig. 22). The details of this three-part partitioning calculation method are described in our previous report [5]. Under the calculation conditions used in this study, the compressibility is low even near the spout, so incompressible calculations were also performed in the first part.

Based on the calculation method described in Section 4, the spouting position for the first part was set 20 mm above the experiment position. In addition, the k-ω SST model that can accurately calculate jet turbulence was used as the turbulence model. Piping is present in the analysis region for the second part, so the unsteady-state calculation results were averaged, using the steady-state calculation solutions as the initial values. Here, the RSM model was used as the turbulence model. The flow along the wall surface accounts for most of the third part, so the RSM model was used as the turbulence model in the calculations.

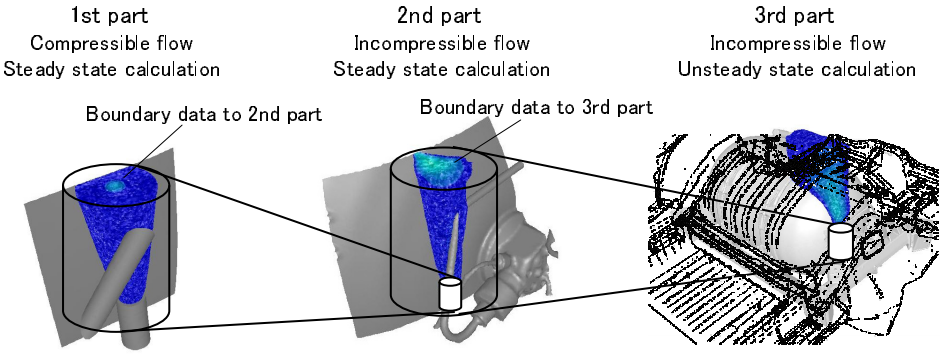

Figure 22. Three parts partitioning method

5.3 Results of Verification

Figure 23 shows contour diagrams of the hydrogen concentrations calculated for each region in the three-part partitioning calculations. The calculation results for the third part enabled visualization of the flow behavior as the hydrogen diffused. Figure 24 compares the calculation results and measured values at the hydrogen concentration measurement position. These data were corresponding well. This confirmed that the calculation methods determined based on the results in Section 4 are effective even for complex vehicle shapes. In addition, the total calculation time from the first through the third part was approximately four days, which verified that calculations can be performed in a practical time, even in investigations of FCEV design.

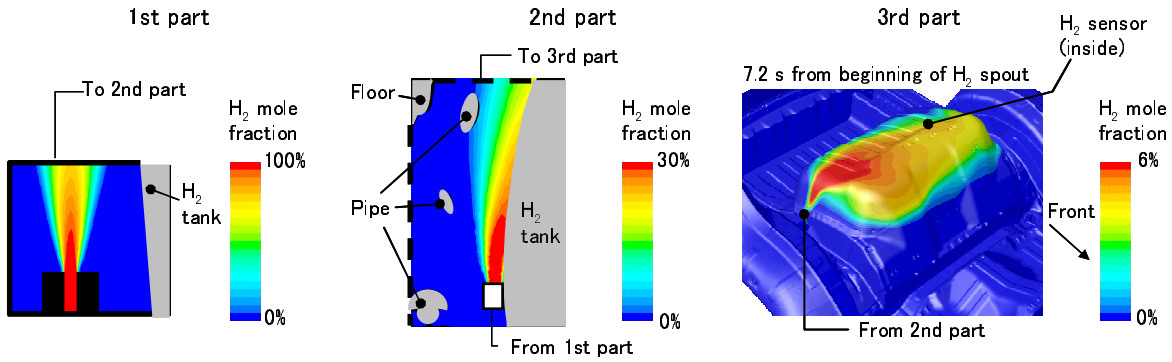

Figure 23. Hydrogen mole fraction contours

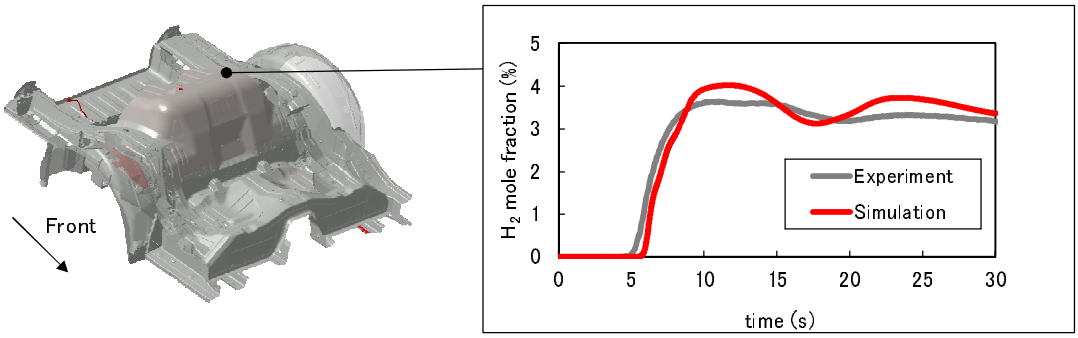

Figure 24. H_2 mole fractions at sensor position

6. CONCLUSION

The turbulence elements that should be taken into account when calculating the diffusion of hydrogen in the vehicle underfloor space were classified into the three types of jet flow, wake flow, and wall turbulence. The characteristics of each flow type were understood through experiments, and appropriate calculation methods were introduced.

(1) Jet flow from a spout transitions from laminar flow to turbulence at a Reynolds number of around 1500. The conditions that result in turbulence can be accurately calculated using the k-ω SST model.

(2) Wake flow involves large wavering, and steady-state calculations underestimate the effects of hydrogen diffusion due to turbulence. Calculations that include the effects of wavering can be performed by unsteady-state calculations using the steady-state calculation results as the initial values.

(3) The flow along a wall surface spreads widely in the direction parallel to the wall surface due to wall turbulence. This can be accurately calculated using the RSM model.

Comparison with measured values verified that these calculation methods can be used to accurately calculate hydrogen diffusion, even in complexly shaped vehicle underfloor spaces.

In the future it is hoped that this simulation technology will be applied to the development of FCEV and other hydrogen energy technology, and help to realize a safe hydrogen society.

7. REFERENCES

1. Nohmi, T., Maekawa, M., Mogi, T., Suiso Ion Sensa, *Suiso Enerugi Sisutemu*, **33**, No.2, 2008, pp.54-59. (in Japanese)
2. New Energy and Industrial Technology Development Organization, Suisono Yukoriyou Gaidobukku, 2008, p.554-561. (in Japanese)
3. Utanohara, Y., Nakamura, A., Nagaya, Y., Murase, M., LDV measurements and URANS calculations downstream of a globe valve, *Institute of Nuclear Safety System Journal*, **17**, 2010, pp.88-103. (in Japanese)
4. Miyake, Y., Vortices in Near Wall Turbulence, *Nagare*, **22**, 2003, pp.29-34. (in Japanese)
5. Matsumoto, M., Shimizu, K., Research of Simulation Method of Hydrogen Diffusion for Fuel Cell Electric Vehicle Development, *Honda R&D Technical Review*, **23**, No.1, 2011, pp.58-64.